Technical University of Denmark

DTU

Detecting and identifying damage in sandwich polymer composite by using acoustic emission

McGugan, Malcolm; Sørensen, Bent F.; Østergaard, R.; Bech, T.

Publication date:
2006

Document Version
Publisher's PDF, also known as Version of record

Link back to DTU Orbit

DTU Library
Technical Information Center of Denmark

Risø-R-1580(EN)

Detecting and identifying damage in sandwich polymer composite by using acoustic emission

Malcolm McGugan, Bent F. Sørensen, Rasmus Østergaard and Thomas Bech

Risø National Laboratory
Roskilde
Denmark
December 2006

Forfatter: Malcolm McGugan, Bent F. Sørensen, Rasmus Østergaard and Thomas Bech
Titel: Detecting and identifying damage in sandwich polymer composite by using acoustic emission
Afdeling: AFM

Resume (max. 2000 char.):

Acoustic emission is a useful monitoring tool for extracting extra information during mechanical testing of polymer composite sandwich materials. The study of fracture mechanics within test specimens extracted from wind turbine blade material is presented. The contribution of the acoustic emission monitoring technique in defining different failure modes identified during the testing is discussed. The development of in-situ structural monitoring and control systems is considered.

Key words: acoustic emission, mechanical testing, polymer, composite, sandwich, fracture mechanics, wind turbine blade, failure mode, structural monitoring.

Indhold

Foreword

This report is the first of two milestone reports contained within Work Package One (WP1) of the project. A complete description of the project structure and deliverables is contained within the project application document [1] and the technical appendix [2].

In WP1, laboratory experiments involving acoustic emission (AE) sensors have been carried out on polymer composite sandwich material extracted from a wind turbine blade.

The testing involves the characterisation of AE sensor signals emitted during damage propagation within small sandwich composite specimens exposed to crack opening loads. The location of the crack influences the characteristics of the sensor output. The "severity" of the damage is judged using only the AE signals by relating the characteristics of the sensor output to the energy required for crack growth according to basic fracture mechanics of sandwich structures.

However, the initial section of this report introduces the reader to various basic techniques and ideas involved in acoustic emission sensing for structural health monitoring.

The attached appendix summarises the work of DEMEX in generating the orthotropic localisation algorithms necessary to locate AE events on a non-isotropic composite material.

Introduction to acoustic emission principles and techniques

Introduction to Acoustic Emission

When certain dynamic processes occur rapidly in or on the surface of a material some of the energy that is released generates elastic stress waves; we might say vibrations. These stress waves propagate from the source and can be detected by sensitive transducers. The signal from these transducers (once amplified) is then available for analysis. Information about the location, severity and nature of the event causing the stress wave emission can be deduced from the received signals. [3]

When loaded, composite materials in a structure emit a great deal of these transient stress waves as a result of non-reversible micro damage events such as matrix cracking. This multitude of small-scale events is detectable long before a reduction in structure stiffness and/or the appearance of visible (macroscale) cracking. Where a composite structure has sustained damage (as the result of an impact for example), there is a great deal more stress wave emission activity from this area during loading, than from the surrounding "good" material. [4]

The potential exists, therefore, to locate defects and damaged areas in composite structures, before they become threatening to the structure integrity, by monitoring these transient stress waves. As the signal generally does not fall in the human audible range, the term acoustic emission (AE) is a misnomer and the alternative term stress wave emission (SWE) would be a more accurate description of the phenomenon, both are used but acoustic emission is the expression in more widespread use.

Where AE sensors are detecting activity from a loaded composite structure, this is known as *passive* sensing. However it is possible to generate an artificial source of stress waves (such as a piezoelectric crystal or a Hsui-Neilsen source) and examine how these signals interact with the transmission material and any defects it contains. This is known as *active* sensing. When a system utilises both modes of operation, this is known as *Acoustoultrasonics*. [5]

Wave propagation

The AE waveform at the source (whether artificial or not) is generally a simple, broadband step or pulse. But the detected signal is invariably far more complex in form, being largely shaped by wave propagation effects between the source and the sensor. This is important to bear in mind as it infers that deconvolution of a received signal will provide a great deal of information regarding the material that the waveform has travelled through, including the presence and severity of any damage.

Wave modes and wave velocity
Wave velocity is a key parameter in AE monitoring, particularly with respect to source location calculations. Different wave modes (compression, shear, surface, flexural, etc.) travel at different velocities and these wave velocities depend on the material and (for some wave modes) the thickness of the material. An average figure that is often assumed for composite materials is 2000m/s. [6]

Wave velocity can be measured by putting a wave pulse into a structure and measuring the time it takes to arrive at a distant sensor. An oscilloscope can be used to capture the waveform at different distances from the source.

Attenuation
As a wave travels, its peak amplitude diminishes. This means it will be harder to detect sources at a greater distance from the sensor. The three most important causes of attenuation are,
(a) geometric spreading of the wavefront,
(b) absorption or damping in the propagating medium and
(c) "leaking" of the wave energy into adjacent media, such as a fluid.

The effect of geometric spreading is easily modelled, the amplitude falls off inversely with distance in "three dimensional" media such as a concrete block or inversely with the square root of distance in "two dimensional" media such as a plate. This type of attenuation is the dominant one close to the source.

Based on absorption or damping in the propagating medium, the amplitude falls off exponentially with distance. This effect is the dominant one far from the source and so fixes the limit of detectability for any given system. The rate of fall off is a material property and also depends on the frequency component of the signal. A figure often assumed for composite materials is 10dB/300mm [6]. The higher the frequency, the higher the attenuation rate, in rough proportionality (see *frequency effect*).

Attenuation due to "leaking" of the signal occurs at structural discontinuities and boundaries. When a signal hits such a discontinuity or boundary a certain amount of the energy is reflected. The amount of energy reflected depends on the geometric and material mismatch at the reflecting boundary.

Frequency effect
Sensors for detecting stress waves can often be classified into two sets;
- *Broadband* transducers that respond to all the frequencies of the stress wave and return a signal which closely replicates the small-scale motion of the surface, and
- *Resonant* transducers that are left undamped and free to "ring" at their resonant frequency (or frequencies).

One of the factors that affect the attenuation rate of a stress wave in materials is the frequency of the transmitted signal. At their source, many signals are broadband (containing a range of frequencies), however the material quickly attenuates the higher frequency ranges, whereas the lower frequency components can travel much further.

In this way it is possible to choose a resonant sensor that "rings" at a high frequency (eg.300kHz) in order to exclusively study local stress wave phenomenon, as sources from further away (such as unwanted noise) will quickly attenuate below detectability. Conversely a sensor resonant at a low frequency (eg.60kHz) will have a far greater sensoric range and can thus "cover" a larger volume of the structure. The drawback will be a greater risk of "noise" sources in the final data set.

Thus the choice of sensor often comes down to an operator decision to trade sensoric range against noise countermeasure.

Effect of damage on wave propagation

Damage present in composite material will interact with transient stress waves [7]. This interaction will influence the shape of the waveform received at the sensor. The type of damage and its level of severity will also influence the waveform.

For example, the flexural wave mode will interact most strongly with damage lying normal to the plane of the wave propagation (delamination, skin/core debonding, etc.) The compression wave mode will interact most strongly with damage lying perpendicular to the plane of wave propagation (matrix cracks/splitting, gouging, core crushing, etc.). If these two effects can be recognised in the received AE waveform then it would be possible to discriminate between damage types.

The presence of damage in a composite material increases the rate of attenuation expected for that material. This is due to structural discontinuities within the damage area dispersing the waveform energy. The greater the area of damage, the more the attenuation rate is affected. Recognising this effect in the received AE waveform would make it possible to judge damage severity.

The frequency distribution of the received waveform is also likely to be affected by the presence and size of various damage types. The absorption rates for different materials vary across the frequency spectrum of the stress wave. The presence of damage in the wave path will result in an altered frequency distribution in the received waveform.

Data harvesting

There is a great deal of information about the source event and the transmission material that can be extracted from an AE waveform. However, there are so many variables affecting the signal that it can be a significant effort to deconvolute these external influences and highlight the key information.

AE technology has been identified as a key research area in America [8], Europe [9] and Japan [10]. Therefore, laboratories all over the world have invested in powerful computers and expensive equipment in order to study specific AE effects in small specimens. This fundamental research is required to establish a good understanding of the complex topics involved.

The laboratory work involves simple test specimens with close control over as many variables as possible. In a practical structure there is a huge increase in the complexity and using the techniques successfully developed in the laboratory becomes impossible without supercomputer processing power, e.g. Los Alamos [8]. This means data analysis is not conducted in "real time" and the process becomes unwieldy.

The challenge of data harvesting (extracting useful information efficiently from a sea of available data) has been repeatedly highlighted by one of the most respected voices in Structural Health Monitoring research, Prof. Fu-Kuo Chang [11]. Chang predicts that the most successful system to come out of the current world-wide research effort will be one based on novelty detection. That is, a system that does not attempt to interpret the entire data stream, but only marks deviations from the normal signal profile. Such a system would focus only on one or two key indicators within a signal waveform and thus save processing requirement and permit real time operation.

Active AE systems

Devilliers et al. [12] and Osmont et al. [13] have published work on using an active AE system to detect the presence of damage/defects in sandwich composite panels. They used wave propagation theory to calculate optimal signal frequencies and sensor resonance and predicted that the functional mode component of any transmitted stress wave would interact with areas that contained skin/core debonding.

A sandwich panel was fabricated from which a section of core was then removed. A stress wave source and receiver were positioned as shown in figure 1 and the two waveforms compared.
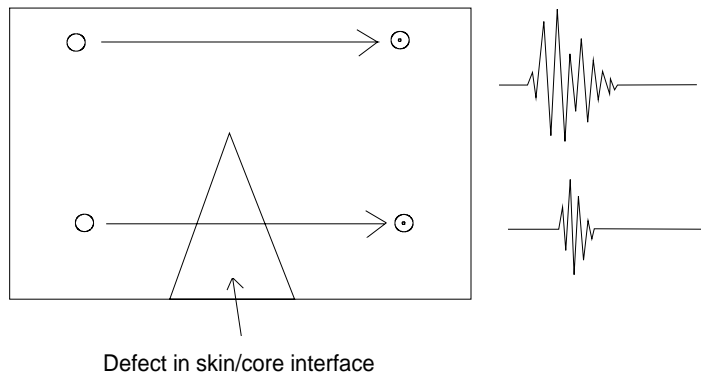

Defect in skin/core interface

Figure 1: Effect of defect on stress wave propagation between transmitter and receiver

In the first case (template signal) the transmission path is entirely through "good" material. In the second case the transmission path includes an area where there is no core/skin interface. The distances between the source and receiver are identical in each case. The signal received was seen to be affected by the presence of damage and the experiment was declared a success.

Structural Health Monitoring systems based on active AE sensing are not uncommon in aerospace technology demonstrator programs [7],[14]. The sensor/transmitters are mounted on (or embedded within) the structure and during operation they are used to generate waveforms. These generated waveforms are then compared with "template" waveforms that were previously generated by the system, usually shortly after installation.

Differences between the operation generated waveforms and the templates are intended to be indicative of the presence of damage between the transmitter and the receiver [12], [13].

However, a serious problem with this approach is the number of other factors that affect the wave propagation in the material and which cannot be easily controlled away from laboratory conditions. Factors such as ambient temperature, water content, background noise, material age effects, structure operation, etc. The result is that the generated waveforms differing from the template were often due too factors other than the presence of damage.

Mobile transmitter/receiver set up

In order to circumvent this problem it is necessary to either deconvolute the effect of these other factors from the received waveform or to create a data normalisation; where the so-called "template" signal takes account of these other factors every time the system is used and can still detect damage as a novelty event.

A linked transmitter/receiver unit that is swept across an area to be scanned will return a waveform based on the wave propagation effects that exist in the material at that time. Reinforcement lay-up, material type, material age, water content, ambient temperature, transmitted signal, receiver frequency response, background noise, etc. If these conditions are constant along the length material and for the duration of the sweep then no significant difference in the waveform will be observed (fig.2).
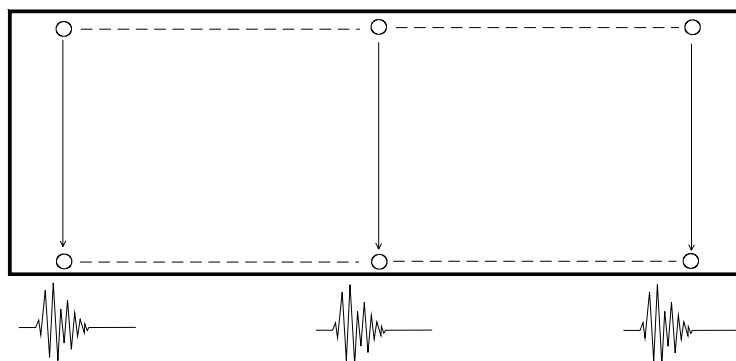
Figure 2; Active AE scan of an undamaged panel

If, however, there is a novelty detected along the length of the sweep then the waveform received will be altered at that area (fig.3). This novelty in the signal waveform could be due to the *known* presence of structural stiffening or a repair perhaps, or an *unknown* novelty which would include areas containing damage.
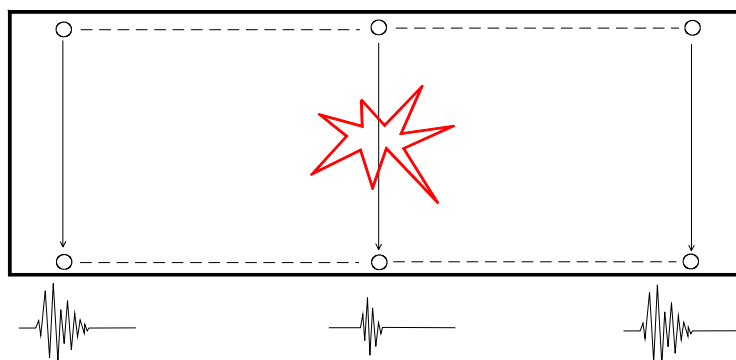
Figure 3; Active AE scan of a panel containing a damaged area

Detecting damage in a wind turbine blade structure

At Risø National Laboratory, a simple technique for rapidly establishing the extent of skin debonding in large wind turbine blades has been developed. The technique is based on active AE sensing and has been used during full scale structural testing [15]. Modern wind turbine blades are large, complex sandwich composite structures that can be as large as 50m long and weigh 50 tonnes.

The sensoric range of AE sensors positioned along the length of the central load bearing spar is established using a Hsui-Neilsen source. The sensoric range of each sensor is determined by the attenuation rate of the material surrounding it. Areas of the structure with poor skin/core bond quality will have a far greater attenuation rate and hence a lower sensoric range. The sensoric range data thus obtained correlates well with bond quality along the length of the structure and can be used to quickly identify areas of damage. These areas can then be inspected in more detail with visual and ultrasonic techniques.

The following diagram (fig.4) shows a schematic of a blade with sensors positioned along the central spar. By plotting the relative sensoric range of each sensor against its' blade position, a good indication of the relative bond quality along the blade is established.
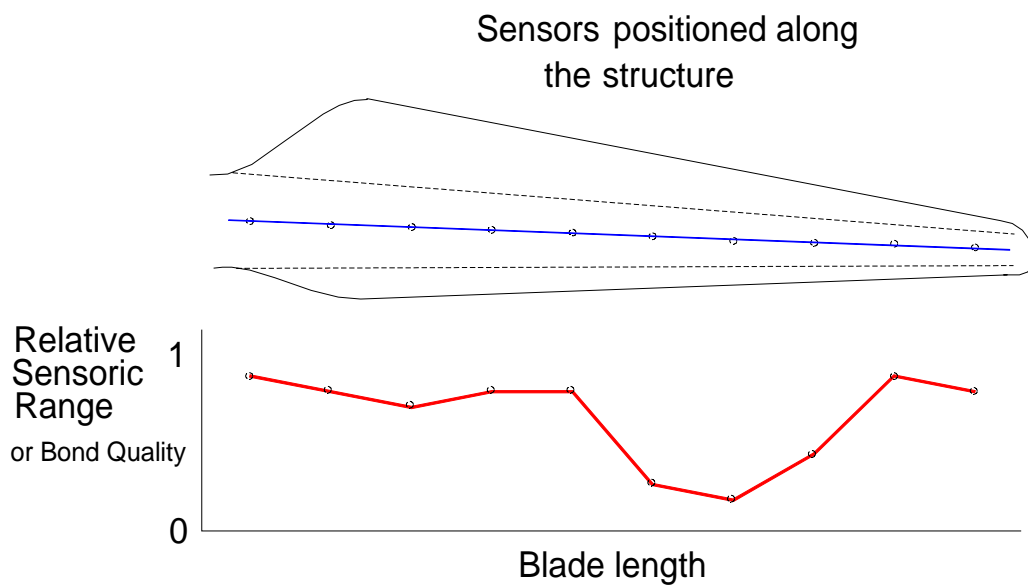

Figure 4; Areas of debonding indicated by the low relative sensoric range of sensors

Passive techniques

Background

In the previous project [16], AE sensors in passive mode were shown to detect the development of many different damage types associated with structural failure in glass reinforced plastic (GRP) wind turbine blades. One of the goals of the current project [1] [2] is to highlight the possibility of distinguishing between the different signals generated and thus identify a specific damage type using sensor data alone.

One very significant damage event in sandwich composite materials is skin/core debonding, where the exterior layer of laminated composite material becomes detached from the lightweight core material. Once initiated, such damage has the potential to grow quickly and compromise structural performance. The speed at which this damage grows depends on many material and structural factors such as where the damage is located in the structure, how large it is, the external loading, the material quality and so on. [17] Clearly one of the most significant factors determining the growth rate is the energy uptake required to advance the crack front.

The interface between skin and core in a sandwich composite structure is often characterised as a "resin rich layer", where there is little or no reinforcement of the polymer resin matrix by the glass or carbon fibres. Consequently, if damage is initiated between the skin and core, the energy uptake required to propagate the damage through this layer is low. This is known as *debonding* of the skin from the core.

There is a laminated structure within the skin material formed by the layers of fabric reinforcement held in place by the polymer resin matrix. Damage can also form between two layers of the composite material and this is known as *delamination*. By comparison with skin/core debonding however, there is likely to be far more fibre reinforcement between two laminate layers in the skin material itself than there is between the skin and core. This *fibre bridging* between skin laminate layers is the reason that the energy required to propagate a delamination is generally far greater than the energy required to propagate a debond.
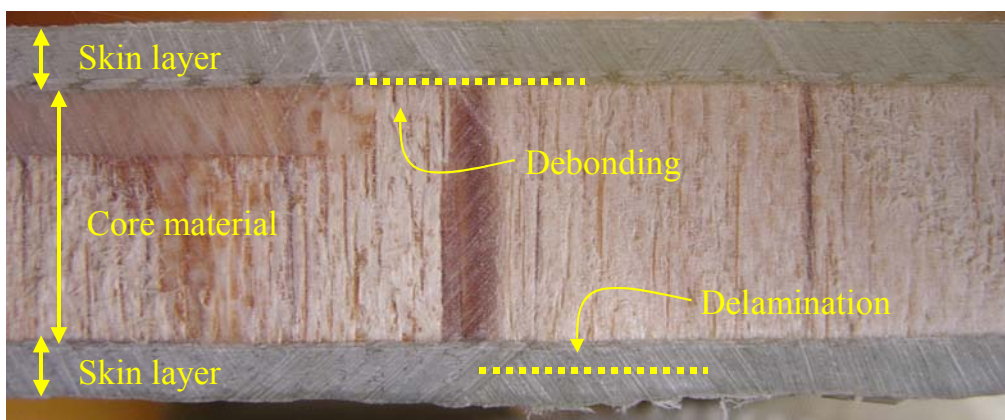

Figure 5: A typical sandwich composite cross section, with potential debonding and delamination sites indicated.

Damage of this kind (both delamination and debonding) has traditionally been detected during routine inspection using non-destructive techniques such as pulse echo ultrasonic inspection. However, such an inspection is not always able to distinguish between debonds and delaminations [18] as both create a similar "loss of transmission" in the returned ultrasound signal and the difference in depth between a possible debond or delamination can be a matter of millimetres.

Over time, there has been an adoption of damage tolerance approaches to the maintenance of large GRP structures, in order to extend service life and to avoid invasive repair procedures. A successful damage tolerance assessment requires detailed information, including the energy uptake of the damage. These two paths of crack advance (debond and delamination) have significantly different fracture resistances. Obviously this difference has a critical influence on any damage tolerance assessment based on fracture mechanics, therefore, distinguishing between a debond and a delamination becomes necessary.

Basic Fracture mechanics for sandwich polymer composites

The high stiffness to weight ratio of FRP sandwich panels, and the ease with which this stiffness can be predicted, has contributed to their popularity. More complex is the relationship between the growth of damage/defects in the skin (or skin/core interface) and shear stresses in the panel.

Risø has a considerable expertise in the investigation of fracture mechanics, and has hosted many laboratory investigations using different materials and carefully controlled loading conditions. Sensor technology (including AE) has been used on test specimens to assist the understanding of damage initiation and growth, and to assist in the characterisation of crack type and energy uptake.

Cracking of FRP sandwich structures occurs along weak planes. In fracture mechanics terms, cracking is mixed mode; both normal and shear stresses are present at the crack tip. The relative amount of shear stress to the normal stress is usually expressed by the mode mixity, ψ [19]. Furthermore, for a given crack plane, the fracture resistance can depend on the mode mixity

For sandwich structures, crack propagation can occur by three fundamental different failure modes, see Figure 6. These are (a) delamination (cracking along a weak plane in the laminate), (b) debonding (cracking along the skin/core interface) and (c) crack growth in the core material (e.g. as sub-interface cracking).
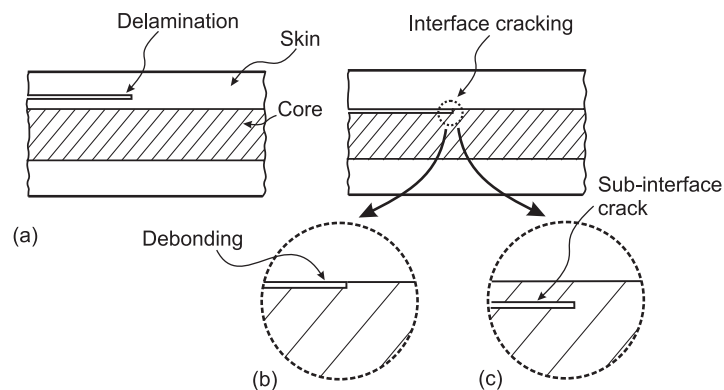

Figure 6. Basic cracking modes in sandwich structures: (a) cracking in the skin, (b) interface debonding and (c) cracking in the core material.

It is important that one is capable of distinguishing between these failure modes, because the resistance to fracture can be very different for the different cracking planes. It follows that the severity of a crack in a sandwich structure does not only depend on the crack size, but also at its position through the thickness of the sandwich

A criterion for delamination crack growth is that the energy release rate reaches a critical value, the fracture energy of the delamination front, J_0^d (superscript d indicates delamination). In some sandwich systems, delamination is accompanied by crack bridging (fibres or fibre bundles that connect the crack faces). The crack bridging can result in a substantial increase in the fracture resistance. Then, the initial delamination resistance, J_0^d, (i.e. of a crack with no fibre bridging) and the steady-state fracture resistance, J_{ss}^d, (i.e. of a fully-developed bridging zone) can be taken as material properties.

Fibre bridging can also accompany skin/core debonding. Thus, the initial and the steady-state interface fracture resistance, J_0^i and J_{ss}^i, are assumed to be material properties (superscript i indicates interface).

Cracking in the core material is characterised by the fracture energy of the core material, J_c^c (superscript c indicates core). Usually, a crack in a homogenous body selects a path perpendicular to the largest principal stress (a pure mode I path) [20]. However, there may also be cases where cracking occurs as mixed mode cracking of a sub-interface crack. This is expected when (1) the crack is positioned inside the core and the mode mixity is such that the crack is driven towards the skin/core interface and (2) the fracture resistance of the core material is much lower than that of the interface, $J_c^c << J_0^i$. In practice skin layers are often bonded to the core, so there may be a resin rich zone at the interface. If the resin-rich zone possesses a higher fracture resistance than the pure core material, cracking then takes place just outside the matrix-rich zone.

Test Procedure

The test specimen used in this study is a double cantilever beam specimen loaded with uneven bending moments (DCB-UBM). The geometry and loading is shown schematically in figure 7, and in a photograph in figure 8.
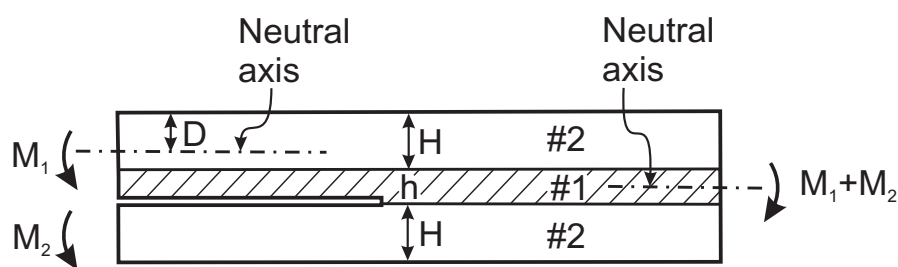
Figure 7. Geometry and loading of a DCB-UBM sandwich specimen.
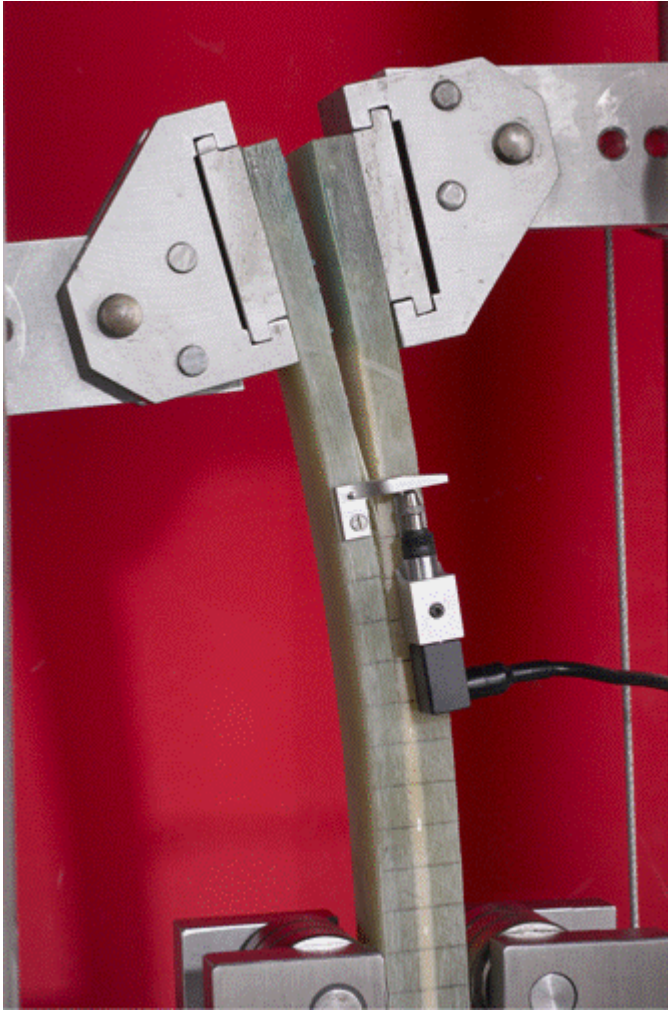
Figure 8. Photograph showing the loading of a typical DCB-UBM specimen.

The crack energy release rate is determined by evaluating the path-independent J integral along the external boundaries. For plane strain the result is [17].

$$J_{\text{ext}} = \frac{1-\nu_2^2}{B^2 H^3 E_2} \left\{ \frac{M_1^2}{2\eta^3 I_0} + 6M_2^2 - \frac{(M_1+M_2)^2}{2\eta^3 I_1} \right\}, \qquad (1)$$

where M_1 and M_2 denote the applied bending moments (positive signs are shown in the figure), H, E_2 and ν_2 denote the thickness, the Young's' modulus and the Poisson's ratio of the skin layers (material #2). B is the specimen width. For plane stress, the terms $1-\nu_2^2$ should be replaced by unity. The dimensionless parameters I_0 and I_1 are given by [21]:

$$I_0 = \frac{1}{3}\frac{1}{\eta^3} - \frac{\Delta}{\eta^2} + \frac{\Delta^2}{\eta} + \Sigma\left(\frac{1}{\eta^2} + \frac{1}{\eta} + \Delta^2 - 2\frac{\Delta}{\eta} - \Delta + \frac{1}{3}\right);$$

$$I_1 = \frac{1}{12}\left(\Sigma + \frac{8}{\eta^3} + \frac{12}{\eta^2} + \frac{6}{\eta}\right) \quad (2)$$

and

$$\eta = \frac{h}{H} \; ; \qquad\qquad \Sigma = \frac{E_1}{E_2}\frac{1-\nu_2^2}{1-\nu_1^2} \; ; \qquad\qquad \Delta = \frac{D}{h} = \frac{1+2\Sigma\eta+\Sigma\eta^2}{2\eta(1+\Sigma\eta)} \; . \qquad (3)$$

Here, E_1 and ν_2 are the Young's' modulus and Poisson's ratio of the core (material #1) and D denotes the position of the neutral axis of the bimaterial beam (measured from the top of the skin layer). For plane stress $\Sigma = E_1/E_2$. Equation (1) is valid for both small-scale failure process zone and for large scale bridging problems.

The crack tip stress state is described in terms of the mode mixity, ψ, which is a measure of the amount of shear and normal stress at the crack tip. The mode mixity can be obtained from the numerical study of Østergaard and Sørensen [21]. With the geometry fixed, the mode mixity can be varied by altering the ratio between the applied moments, M_1/M_2. The mode mixity affects the path the crack selects. It is thus possible, by varying the ratio between the moments to control where cracking occurs (along the core/skin interface, into the core or into the skin).

The principle of creating different bending moments in the two free beams of the DCB-UBM specimen is shown schematically in figure 9 and as an example specimen in the test rig in figure 10. Forces of identical magnitude, P, are applied perpendicular to two transverse beams connected to the end of the beams of the DCB specimen. Identical forces are obtained by the use of a wire arrangement. The uncracked end of the specimen is restricted from rotation but can move freely in the x_1-direction. Different moments are obtained if the length of the two moment arms, ℓ_1 and ℓ_2, of the transverse beams are different. The applied moments are $M_1 = P\ell_1$ and $M_2 = P\ell_2$. It follows that the mode mixity can be changed simply by altering one moment arm, say ℓ_1.
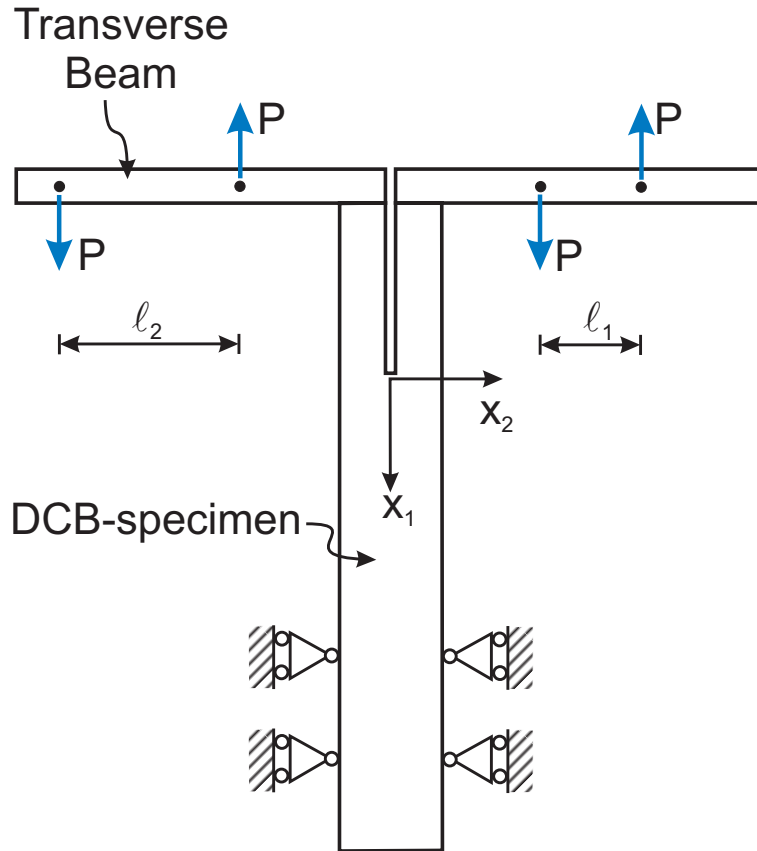

Figure 9. Schematic of the proposed loading method; the mode mixity is controlled entirely by altering the length of one of the transverse beam arms, e.g. ℓ_1.
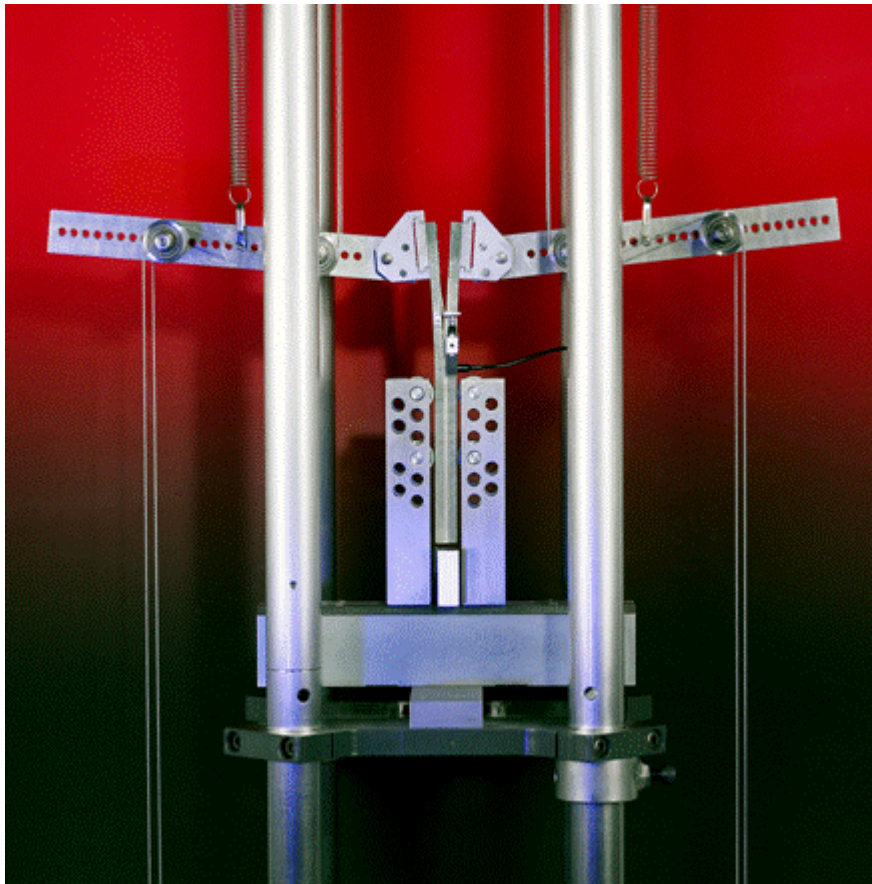
Figure 10.Photograph showing the test rig loading method; the mode mixity is controlled entirely by altering the length of one of the transverse beam arms.

Test one: Materials and sensors

In the initial set of tests covered by the WP1 project investigation, three identical DCB specimens (GRP skins, polymeric foam core) were tested in the way described above. By varying the ratio between the applied moments it was possible to control the type of crack generated during the loading.

AE data was recorded on each test specimen using a two channel SPARTAN AT, PACmicro80 + 1220A preamplifier. The two small sensors were taped to the skin face closest to the crack starter as the specimen was held in the test machine immediately prior to loading. Sensor 1 positioned adjacent to the crack initiator and sensor 2 120mm along the specimen in the direction of the crack growth.

In order to clarify the understanding of the materials crack behaviour under different mode mixity conditions, it was expected that the AE data would highlight damage initiation and location of the crack front during the static loading and subsequent crack propagation in each DCB specimen. The AE characteristics recorded were also expected to reflect the different types of crack generated in the material.

Test one: Results

The three identical test specimens (designated H1309, H1310 and H1311) were loaded in such a way that the crack growth was within the skin/core interface (crack type b. in figure 6). However, by altering the applied moments it was possible to control the degree of fibre bridging present in this debonding, and hence to vary the

energy uptake of the crack between the material values for J_0^i (an interface crack with no fibre bridging) and J_{ss}^i (an interface crack with a fully developed bridging zone). H1311 was loaded in such a way that no fibre bridging was present in the crack (J_0^i), H1309 was loaded in such a way that a fully developed bridging zone was present (J_{ss}^i), and H1310 was loaded at an intermediate ratio (J_0^i<J<J_{ss}^i).

AE data recorded in the three test specimens varied due to the different energy uptake values for the crack growth, both in the general activity during the test and also in the characteristics of the recorded waveforms. Differences in the general AE activity recorded during the tests reflected the type of crack growth taking place in each specimen, see table I.

H1309	J^i_{ss}	• Fully developed bridging zone (lots of fibre bridging) • Huge number of AE hits • Low intensity hits • Controlled crack growth (slow)
H1310	$J^i_{ss>x>0}$	• Intermediate bridging zone • Intermediate intensity • Stable crack growth ("mini-jumps)
H1311	J^i_0	• Crack in resin rich layer (very little fibre bridging) • Few AE hits • Large intensity hits • Crack growth in "jumps" (resin plasticity)

MICROCRACKS

↓

MACROCRACKS
(friction component)
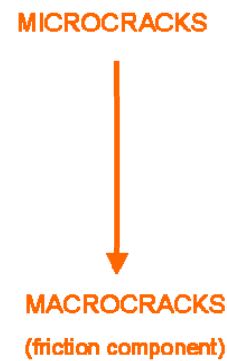
Table I. Summarising the general differences between the crack growth observed in the three identical DCB specimens.

A huge number of low intensity hits were recorded for H1309 (see table II) and the crack growth was controlled and grew only very slowly (see figure 11). By comparison, H1311 had far fewer AE hits but each individual hit contained far more energy (table II). The crack growth here was less stable (due to resin plasticity) and progressed entirely during two sudden "jumps" forward, the AE trace reflected this (see figure 13). H1310 was an intermediate case, an intermediate number of hits, energy per hit and length of test/crack growth (see table II). And although the AE trace (and crack growth) during the test was generally stable, it could be seen from the AE that the crack growth was in fact via a series of "mini-jumps" (see figure 12).

H1309					
AE Hits	36102				
Cum counts	859580	Average NRG/hit	17.08		
Cum NRG	616714	Average counts/hit	23.8	**Av. NRG/count**	**0.718**
Time (s)	415				
H1310					
AE Hits	23853				
Cum counts	530724	Average NRG/hit	22.20		
Cum NRG	529508	Average counts/hit	22.25	**Av. NRG/count**	**0.998**
Time (s)	310				
H1311					
AE Hits	1324				
Cum counts	40589	Average NRG/hit	40.09		
Cum NRG	53083	Average counts/hit	30.66	**Av. NRG/count**	**1.308**
Time (s)	180				

Table II: AE Hit data for the three DCB crack opening tests

H1309 Cumulative Energy

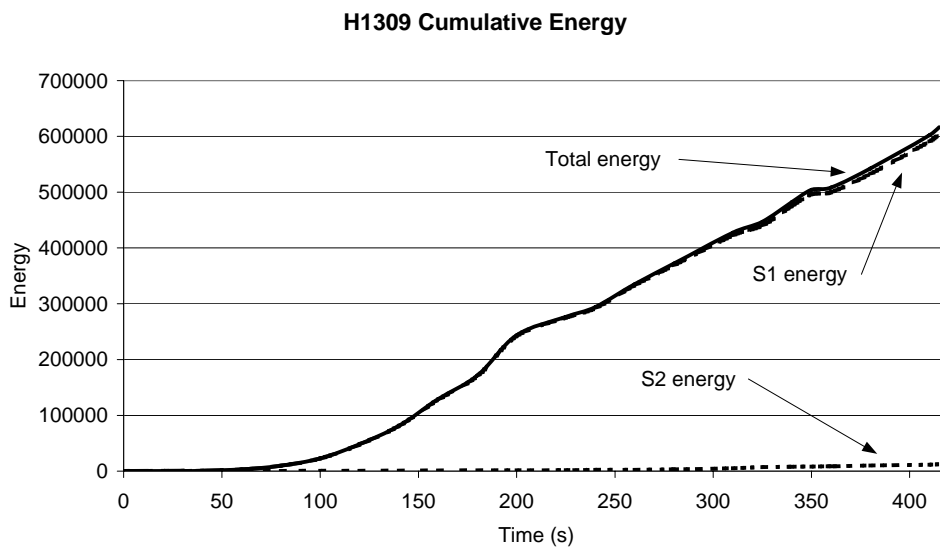*Figure 11. Showing the AE energy recorded on the two sensors during crack growth on specimen H1309 (extensive fibre bridging)*

H1310 Cumulative Energy
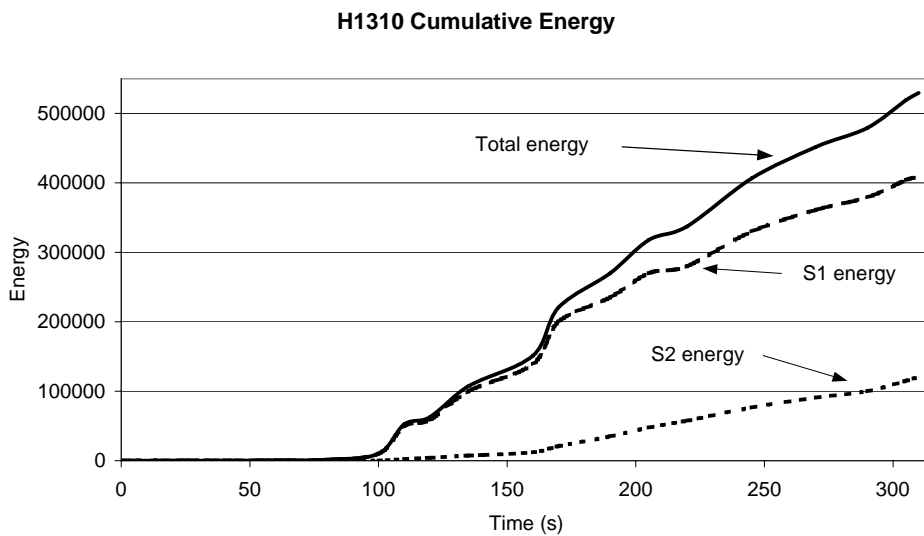

Figure 11. Showing the AE energy recorded on the two sensors during crack growth on specimen H1310 (intermediate case)
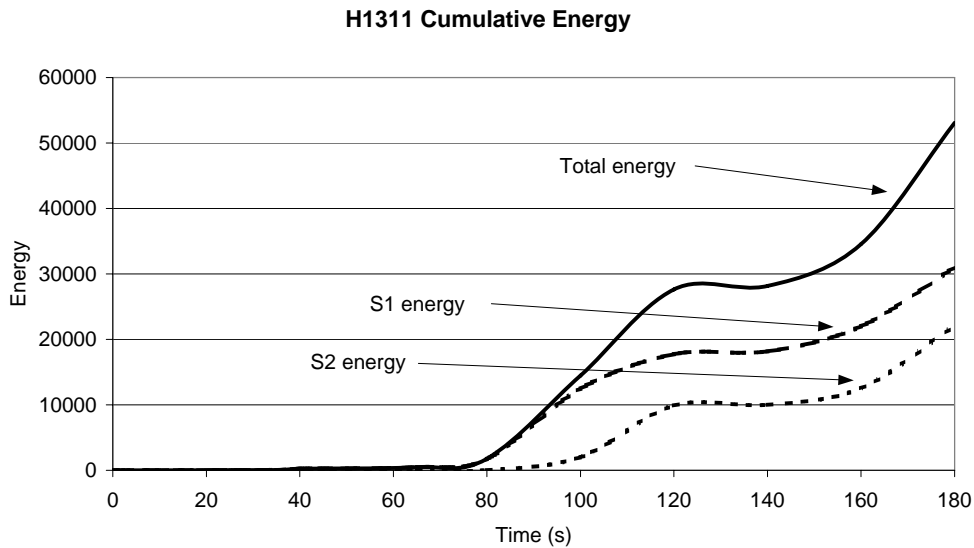
H1311 Cumulative Energy

Figure 13. Showing the AE energy recorded on the two sensors during crack growth on specimen H1311 (no fibre bridging).

Test one: Discussion

The different crack types generated in these three identical DCB specimens created very different acoustric emission profiles.

A key observation is that simply observing total AE activity or cumulated AE energy release is not suficient to determine the "severity" of a defect in a sandwich GRP material. In the graphs and tables contained in the previous section, the crack growth involving fibre bridging (H1309) generates a huge number of AE events, and far more energy is released overall than in the other specimens. However this does not correlate with the length of crack growth in this specimen. More significant is the amount of energy released per event detected, and the energy released per count (a function of the event duration); these figures are calculated in table II.

In addition to the differences in the AE activity levels, it can also be shown that the characteristics of the recorded data are fundamentally different, reflecting the difference in the crack types for the three specimens. In table II, the total number of AE hits recorded for each test is displayed. Also shown is the cumulated counts (number of times the signal crosses the threshold level) and energy (actually a representative value related to the area described by the AE signals waveform curve) for the entire test.

In passive AE monitoring of small specimens, the number of counts recorded for an AE hit is often a good indicator for the length (in time) of that hit. Short AE signals are generally due to microscale events that do not contain a great deal of energy in and of themselves, although there may be a huge number of them. AE signals that continue for a longer period of time (tens or hundreds of microseconds) almost certainly include a friction-based component and can be classified as macroscale events. These types of signals may be less frequent, but usually contain hugely more energy within each single hit and are far more significant for the material structure.

A crack propagation that involves fibre bridging would be expected to have many more microscale AE events than one that does not. The relevant figures for H1309, which has the greatest amount of fibre bridging, and H1311, which has the least, confirms this. The figures calculated for both average count per hit and average energy per hit are highest for the specimen with the lesser amount of fibre bridging.

It is proposed that by calculating a figure for average energy per count during the course of the test, it will be possible to estimate the relative amount of fibre bridging in any similar specimen at any time during the crack growth, lower ratios for average energy per count (corresponding with the loading ratios) indicating a greater degree of fibre bridging. In a DCB test where the crack type changes (from skin/core debonding to skin delamination or vice versa) due to a change in applied moment, it is anticipated that this could be immediately detected by the system in real time using only AE sensor data.
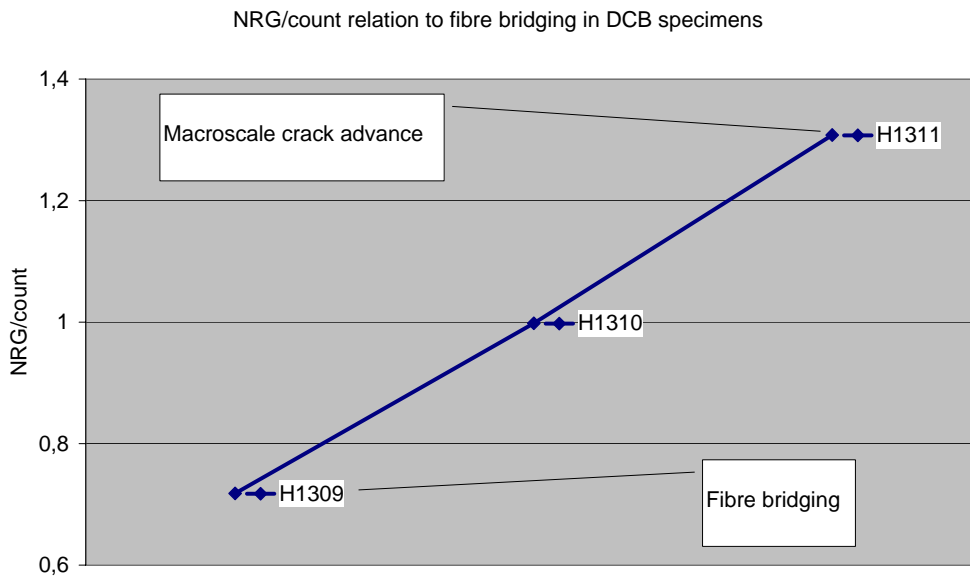
Figure 14. Relationship between energy released per count, and the fibre bridging present in the crack front.

Test Two: Materials and sensors

In the second series of tests covered by the WP1 project investigation, it was decided to investigate the results of the initial testing more thoroughly using wind turbine blade material supplied by Siemens Wind Energy (previously Bonus Energy). From the bulk panel material, two sets of very different DCB specimens were manufactured at Risøs' Composite Materials fabrication laboratory.

Specimen ID	Crack type	Dominant mode	Additional
Dlam01	Delamination crack growth	Mode I	-
Dlam02	Delamination crack growth	Mode I	-
Dlam03	Delamination crack growth	Mode I	-
Dlam04	Delamination crack growth	Mode II	-
Dlam05	Not tested	-	-
Dbon06	Debonding crack growth	Mode I	-
Dbon07	Debonding crack growth	Mode I	-

Dbon08	Debonding crack growth	Mode I	-			
Dbon09	Debonding crack growth	Mode II	Friction			
Dbon10	Not tested	-	-			

Table III; Summary of the second series of DCB specimen testing (material taken from wind turbine blade material)

The first set (*Dlam01-05*) was created entirely from "skin" material and was pre-cracked in such a way as to involve a delamination type crack growth between the laminate plys (see figure 5). The second set (*Dbon06-10*) was created to include a pre-crack at the skin/core interface and thus involve a debonding type crack growth (see figure 5).

AE data was recorded on each test specimen using a two channel SPARTAN AT, PACmicro80 + 1220A preamplifier. The two small sensors were taped to the skin face closest to the crack starter as the specimen was held in the test machine immediately prior to loading. Sensor 1 positioned adjacent to the crack initiator and sensor 2 120mm along the specimen in the direction of the crack growth.

Test two: Results

In both set of testing it was noted which periods corresponded to load increase, steady state crack growth, load hold, unloading, and so on. In this way it was hoped to obtain a better comparison of the relationship between the acoustic emission signals and damage development.

Dlam01	AE hits	CUMcounts	CUM_NRG	NRG/hit	Counts/hit	NRG/count
Total	34494	499067	317569	9.21	14.47	0.64
Load increase	3248	39026	28964	8.92	12.02	0.74
Mode I steady	22500	342839	217067	9.65	15.24	0.63
Load hold	3598	49562	30268	8.41	13.77	0.61
Load increase	5148	67640	41270	8.02	13.14	0.61
Dlam02	**AE hits**	**CUMcounts**	**CUM_NRG**	**NRG/hit**	**Counts/hit**	**NRG/count**
Total	40310	550027	335303	8.32	13.64	0.61
Load increase	8680	109014	68392	7.88	12.56	0.63
Mode I steady	31630	441013	266911	8.44	13.94	0.61
Dlam03	**AE hits**	**CUMcounts**	**CUM_NRG**	**NRG/hit**	**Counts/hit**	**NRG/count**
Total	52785	655875	417985	7.92	12.43	0.64
Load increase	4463	49127	37036	8.30	11.01	0.75
Mode I steady	25130	364196	222725	8.86	14.49	0.61
Load hold	390	5293	3058	7.84	13.57	0.58
Load increase	22802	237259	155166	6.80	10.41	0.65
Dlam04	**AE hits**	**CUMcounts**	**CUM_NRG**	**NRG/hit**	**Counts/hit**	**NRG/count**
Total	15857	196795	137352	8.66	12.41	0.70
Load increase	924	10818	7783	8.42	11.71	0.72
Mode II steady	13852	175403	122745	8.86	12.66	0.70
End decrease	1081	10574	6824	6.31	9.78	0.65
Dbon06	**AE hits**	**CUMcounts**	**CUM_NRG**	**NRG/hit**	**Counts/hit**	**NRG/count**
Total	2705	30523	21546	7.97	11.28	0.71

Load increase	262	1807	1586	6.05	6.90	0.88
Rapid growth	1875	25468	16845	8.98	13.58	0.66
Mode I steady	568	3248	3115	5.48	5.71	0.96
Dbon07	**AE hits**	**CUMcounts**	**CUM_NRG**	**NRG/hit**	**Counts/hit**	**NRG/count**
Total	1911	25975	18316	9.58	13.59	0.71
Load increase	357	4940	3069	8.60	13.84	0.62
Rapid growth	1346	19967	14170	10.53	14.83	0.71
Mode I steady	208	1068	1077	5.18	5.13	1.01
Dbon08	**AE hits**	**CUMcounts**	**CUM_NRG**	**NRG/hit**	**Counts/hit**	**NRG/count**
Mode II loading	24285	201756	155397	6.40	8.31	0.77
Mode I loading	1132	14277	18850	16.65	12.61	1.32
Load increase	660	5207	3975	6.02	7.89	0.76
Rapid growth	22493	182272	132572	5.89	8.10	0.73
Dbon09	**AE hits**	**CUMcounts**	**CUM_NRG**	**NRG/hit**	**Counts/hit**	**NRG/count**
Mode II steady	2511	35167	29329	11.68	14.01	0.83
Friction only	113	654	685	6.06	5.79	1.05

Table IV; AE hit data during the load application for both delamination and debonding DCB specimens under either mode I or mode II crack growth.

Test two: Discussion

Simple scatter plots are routinely used in AE data analysis to distinguish between genuine events and noise events like friction and EMI. See figure 15.
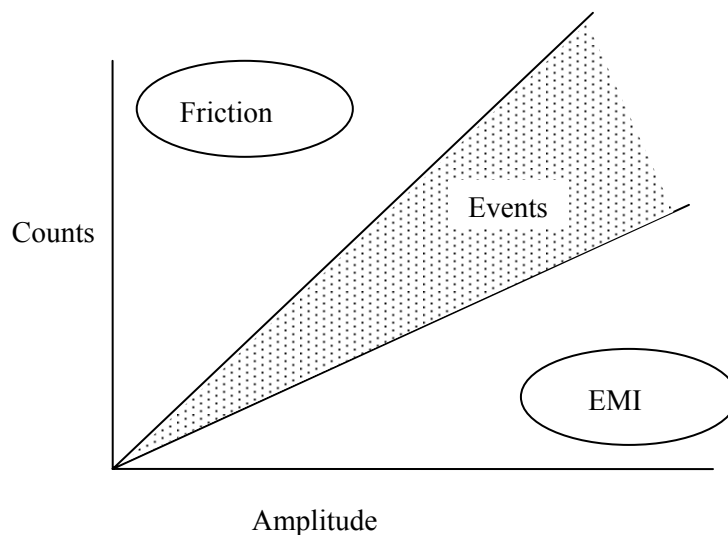

Figure 15. Showing a simple scatter plot used to discriminate real AE events from noise.

Comparing the NRG/hit, Counts/hit and NRG/count values from the different tests, we can check if different damage types (delamination and debonding) and different crack opening modes (mode I and II) produce differences in the AE signals.

The first thing to note from figures 16, 17 and 18, is that there is a huge range of ratios produced during the test caused by increasing and decreasing the bending moment on the loading arms, uncontrolled rapid growth (especially in the debond test specimens), and so on. However, the ratios of most interest are those obtained during the "steady state" crack growth phase.
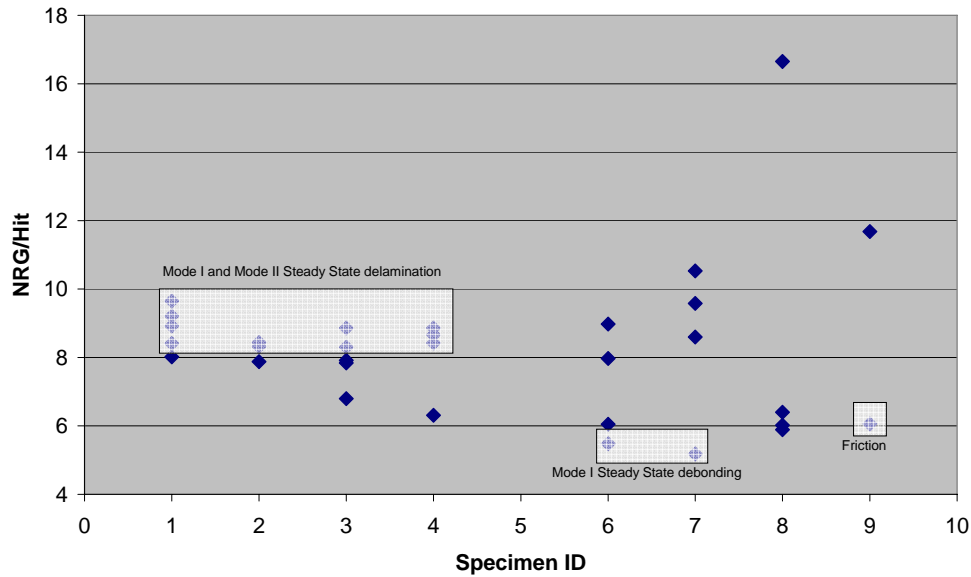

Figure 16. Showing the NRG/Hit ratios for the DCB test specimens
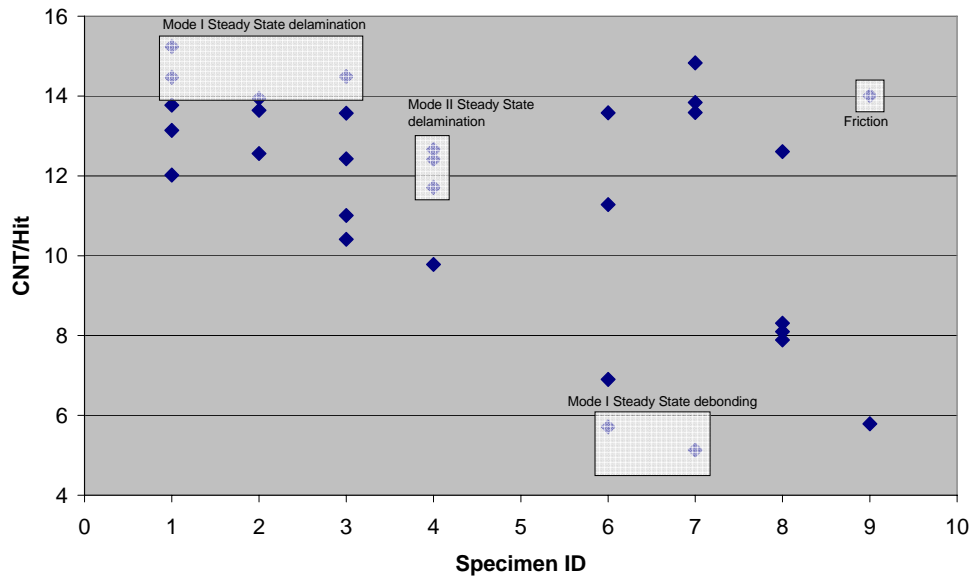
Figure 17. Showing the Counts/Hit ratios for the DCB test specimens

It is also very clear that no single plot can be used to discriminate between the all the different crack growth characteristics we are interested in. For example, in figure 16 there is no difference in the NRG/Hit ratios for mode I and mode II delamination. And although the steady state debonding crack growth shows a much lower ratio, this ratio might be easily confused with friction events.

In figure 17, by comparison, we have a separation between the ratios obtained for Counts/Hit for mode I and II delamination, although both are now close to the ratio for friction. Mode I debonding is well separated.

And in figure 18, there is only a very slight separation between mode I and II delmination, and the well separated debonding is again very close to friction ratio.
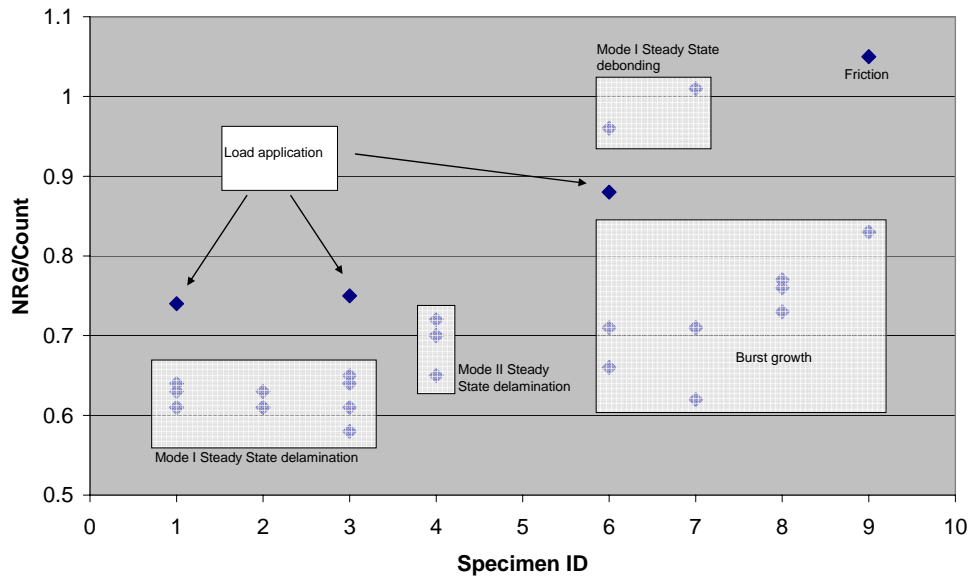

Figure 18. Showing the NRG/Count ratios for the DCB test specimens

Only by considering several aspects of the AE emission simultaneously might it be possible to start establishing patterns that allow identification of an event from its detected AE signal, analysis of this kind are common in research on neural networks.

There is nowhere near enough test data here to begin confirming rules about AE signals variation with source event. However, the ratios do show differences, and these differences, whether due to variations in the amount of fibre bridging or the mode mixity have significant effects on the crack growth rate and hence the "severity" of the crack.

By conflating mode II and delamination with micro (safe) events, and mode I and debonding events with macro (dangerous) events, it may be possible to plot a real time AE activity measurement during our fracture mechanics experiments that will indicate how the specimen is failing, and the point at which AE activity begins to show a deviation from one form of crack growth to another (figure 19). Such information could be used to automatically control the loading arms on a test machine to maintain a certain crack pattern in a specimen, or perhaps even to adjust a structure loading pattern in order to prevent damage (figure 20).
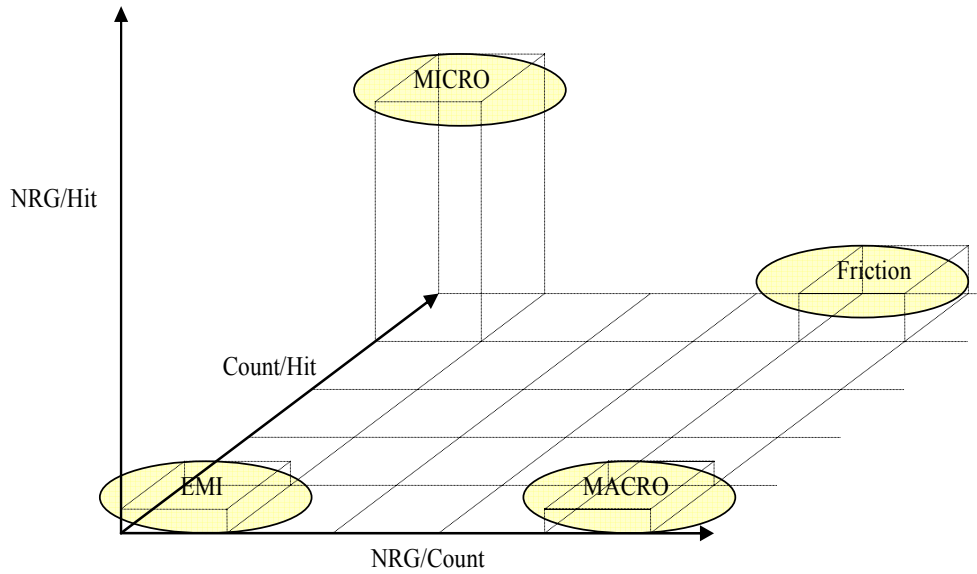
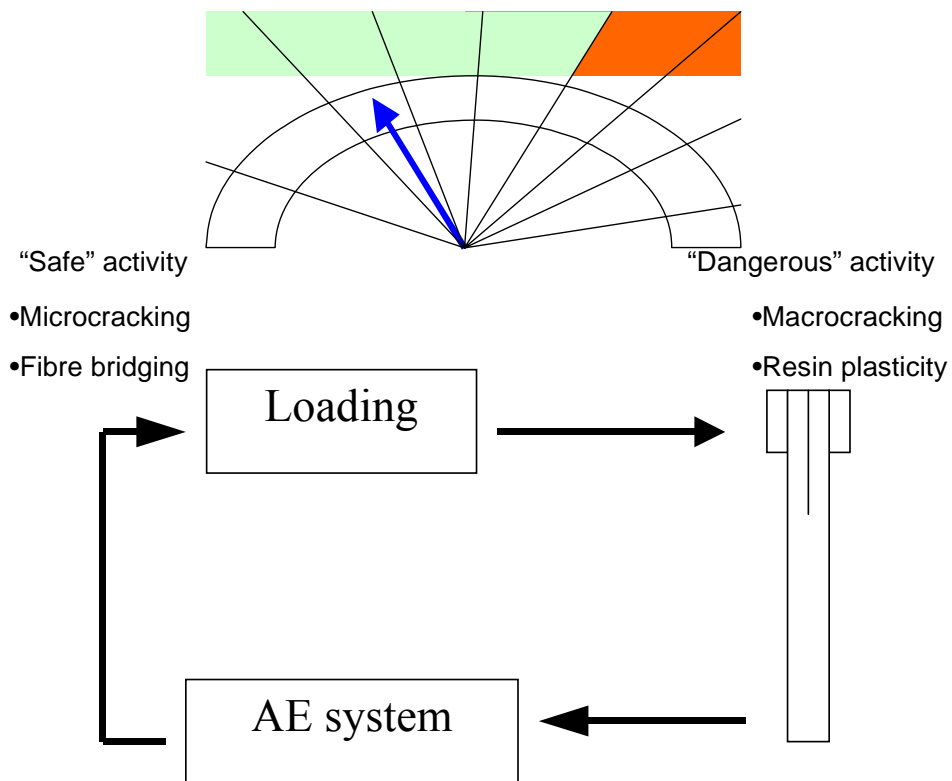*Figure 19. Showing a 3D space with AE activity plotted according to type, compare this with figure 15.*

Figure 20. Showing a feedback control loop for a loaded test specimen (or structure) generated by the detected AE emission.

Conclusion

In the laboratory, AE sensing has been used as an aid to research into fracture mechanics by assisting in identifying the initiation and growth of different crack types in FRP sandwich specimens (foam and solid core). In addition to this, it has been shown that the AE characteristics during crack growth reflect

- the amount of fibre bridging
- the mode mixity
- the location of the crack within the structure
- etc.

Thus the AE signal can be used to indicate the amount of energy required to grow the crack, and hence, judge the crack "severity".

From this it is proposed that an assessment of the crack type present in such a specimen can be made purely on the basis of a sample of the AE data obtained during loading. It is further proposed that any changes in the type of crack occurring during the test can be noted and identified using only the AE record. In this way a "real-time" output during the test would "scale" the crack growth and thus indicate to the test operative whether microscale (fibre bridging) or macroscale crack growth was taking place.

A damage tolerance approach for any structure needs to consider the location of an area of damage, the activity of that damage and the severity of that activity in relation to the particular structural location. One of the key considerations when assessing severity is the energy uptake, how much energy is required to grow the damage. Despite the many practical problems that would require to be investigated, an approach based on AE sensing could be proposed that "rates" the severity of the activity from a particular area of damage in a polymer GRP sandwich panel by comparing the ratio of microscale to macroscale events during in service loading. In this way the energy uptake required to grow the damage could be estimated and the criticality calculated using established laws of fracture mechanics.

Applications for damage assessment sensing include wind turbine blades, where there is a growing interest in establishing such an approach in order to minimise invasive repair activity on detected areas of damage that are not immediately threatening to structural operation.

Sensor data alone has been used to identify the type of crack growth taking place in a polymer GRP sandwich laboratory test specimen. It has therefore been possible to remotely estimate the damage criticality (growth rate) by correlating the signal characteristics to the energy uptake used in standard fracture mechanics.

By monitoring only the AE output from laboratory DCB specimens, it has been possible to discriminate between different types of crack growth within the material. These different crack types have correspondingly different fracture growth rates, and hence their "severity" with respect to damage tolerance assessments for composite sandwich material structures is also different.

References

1. Ansøgningsskema til Elkraft System, PSO-F&U 2003. Grundlag for fjernovervågning af vindmøllevingers tilstand (Fase II: Hovedprojekt), Ordre nr. 103136 – FU3101.

2. Appendix A: Detaljeret projektbeskrivelse. Grundlag for fjernovervågning af vindmøllevingers tilstand (Fase II: Hovedprojekt), Ordre nr. 103136 – FU3101.

3. *McGugan M and Bech T,* Requirements of an AE system for detection of the failure modes in composite materials, MUSEAS I, Multifunctional sensors for structural health monitoring in Aerospace structures, Workshop 2001, CIRA (Centro Italiano Ricerche Aerospaziali), Capua. (Caserta, Italy) November 2001.

4. *Pollock A,* Acoustic emission during loading, Acoustic emission short course, Robinson College - Cambridge. (UK) July 2001.

5. *Rawlings RD,* Acoustic emission and acousto-ultrasonics, Non-destructive testing of composite materials short course, Imperial College (UK). January 1994.

6. *Pollock A,* Spartan AT user's manual, rev 1.1, Physical Acoustic Corporation, Princeton, NJ. (USA) June 1992.

7. *Findlayson RD, Cole P and Lenain JC,* Monitoring ageing structures with acoustic emission and acousto-ultrasonics, Proceedings of the conference on System Identification and Structural Health Monitoring, ed. Güemes JA, pg 601-608, ESTI Aeronáuticos, Madrid. (Spain) June 2000.

8. *Farrar CR,* Los Alamos damage prognosis initiative, Structural Health Monitoring 2002, ed. Balageas D, pg31-45, Paris (France) July 2002.

9. *Pedersen HH,* European commission sixth framework programme, 2nd SAMCO workshop, Brussels (Belgium) October 2002.

10. *Fujino Y and Abe M,* Structural Health Monitoring Research and Development at the University of Tokyo, Structural Health Monitoring 2001, The demands and Challenges, ed. Chang FK, pg61-79, Stanford University, CA (USA) September 2001.

11. *Chang FK,* Ultra reliable and super safe structures for the new century, Structural Health Monitoring 2002, ed. Balageas D, pg3-12, Paris (France) July 2002.

12. *Devillers D, Taillade F, Osmont D, Balageas D and Royer D,* Interaction of Lamb waves with defects in composite sandwich structures, Proceedings of the conference on System Identification and Structural Health Monitoring, ed. Güemes JA, pg 629-638, ESTI Aeronáuticos, Madrid. (Spain) June 2000.

13. *Osmont D, Barnoncel D, Devillers D and Dupont D,* Health monitoring of sandwich plates based on the analysis of the interaction of Lamb waves with

damages, Structural Health Monitoring 2002, ed. Balageas D, pg 336-343, Paris (France) July 2002.

14.   *Balageas D,* Structural Health Monitoring Research and Development at the "European Research Establishments in Aerospace" EREA, Structural Health Monitoring 2001, The demands and Challenges, ed. Chang FK, pg12-29, Stanford University, CA (USA) September 2001.

15.   *Kristensen, O, McGugan M, Sendrup P, Rheinländer J, Rusborg J, Hansen A, Debel C and Sørensen B*, Fundamentals for remote structural health monitoring of wind turbine blades - a preproject. Annex E. Full-scale test of wind turbine blade, using sensors and NDT. Risø-R-1333(EN) (2002) 64 p.

16.   "Fundamentals for remote structural health monitoring of wind turbine blades – a pre-project", Bent Sørensen et al., Risø-R-1336(EN), May 2002.

17.   *Sørensen, B. F., Jørgensen, K., Jacobsen, T. K., and Østergaard, R. C.*, 2004, "A general mixed mode fracture mechanics tests specimen: The DCB-specimen loaded with uneven bending moments", Risø-R-1394(EN), Risø National Laboratory, Denmark.

18.   Private conversations with Jens Rusborg, FORCE technology, Denmark and Kaj Borum, Risø National Laboratory, Denmark.

19.   Hutchinson, J. W., and Suo, Z., 1992, "Mixed mode cracking in layered materials", in <u>Advanced in Applied Mechanics</u>, Vol. 29 (Ed. J. W. Hutchinson and T. Y. Wu), Academic Press, Inc., Boston, pp. 63-191.

20.   Thouless, M. D., and Evans, A. G., 1990, "Comment on the spalling and edge -cracking of plates", *Scripta Metall. Mater.*, Vol. 24, pp. 1507-10.

21.   Østergaard, R. C., and Sørensen, B. F., 2004, "Interface crack in isotropic sandwich structures", Int. J. Fracture. In preparation.

Appendix A

Orthotropisk lokaliseringsystem

Den rapport sammenfatter DEMEX arbejde i PS02 projektet fra August 2003 til Juni 2004.

1. Formål

Det er af stor vigtighed at kunne lokalisere samt detektere en opstået skadestilstand i en vindmøllevinge. Efter almindelige kendte AE metoder til at lokalisere skader, benyttes zone lokalisering hvor den første ramte sensor repræsentere den zone skaden formentlig er opstået i. Denne metode er velegnet til dækning af større områder, men såfremt der opstår en mulig skadestilstand i en zone vil et mere akkurat system være informativt omkring skadesforholdene i området omkring den berørte sensor. En mere nøjagtig lokalisering vil give oplysninger om placering, bruddannelsesmønster, energiindhold i signalet og ud fra dette kan en mere præcis tolkning af skadestilstanden estimeres. Yderligere vil en undersøgelse af selve signalets udseende kunne give en indikation af skadestypen. Dette er dog en meget kompleks problemstilling som rækker ud over projektets rammer.

På denne baggrund har DEMEX i samarbejde med RISØ udviklet et orthotropisk lokaliseringssytem, der kan placere samt estimere skadestilstanden i en vindmøllevinge.

2. Baggrund

En vindmøllevinge består af kompositmateriale med orthotropisk lydudbredelse. Eksisterende trianguleringsalgoritmer er baseret på isotropisk lydudbredelse til anvendelse på f.eks. metaller, men disse algoritmer har ofte en større fejlvisning på kompositmaterialer. Da der samtidigt med projektstarten blev fremlagt en artikel på den 4. internationale workshop for "Structural Health Monitoring", der netop havde udviklet en algoritme, som var istand til at lokalisere AE hits på ortotropiske materialer. Derfor blev det besluttet at programmere algoritmen ind et LabVIEW programeringsmiljø for derved at bruge algoritmen til WP5, fuldskala testen.
Det er ligeledes klart at fremtidige overvågningssytemer må være istand til at håndtere kompositmaterialers specielleegenskaberfor at opnået så præcistbilledeaf strukturenssundhedstilstandsommuligt. .

3. Triangulering

Triangulerings princippet fortæller at der skal 3 tids positioner eller koordinater til at bestemme en lokalitet iplanen. Yderligere er det muligt at bestemme lokaliteter både inden, men også udenfor trekanten somsensorerne danner. Princippet i at tidsforskellen mellem sensoren med den laveste tidskoordinat i forhold til de to andre sensorer, stiller større krav til uddrageisen af tidskoordinaterne for at øge præcisionen. Dette forhold at kompositmaterialer generelt er dårlig til at transmittere lyd samt at signalets "rise time" forøges proportionalt med den vandring som bølgen løber igennem fra undsendelsessted til modtager, gør at "Peak time" triangulering bliver unøjagtig. Maksimal amplituden kan ligeledes skifte top med hvilket menes at lokale ekstremaer kan blive til globale ekstremaer over tid. I disse tilfælde bliver Peak time triangulering umuligt eller misvisende. Derfor er det praktisk at operere med en relativ tidsbestemmelse, der afgøres af forholdet mellem maksimal amplituden samt en passende faktor. Derfor uddrages tidskoordinaten før

signalet når sin maksimale værdi. En høj divisionsfaktor forøger nøjagtigheden, alligevel er der en øvre grænse for hvor stor denne faktor kan være. På grund af kompositmaterialets store dæmpningsevne vil signalets maximal amplitude kunne reduceres med en op til en faktor 1000 på 100cm vandring. Dette medfører at såfremt divisionsfaktoren bliver for stor vil tidsuddragningen kunne ske på en tilfældig støj transient ved et meget lavt signal.

Den orthotropiske algoritme
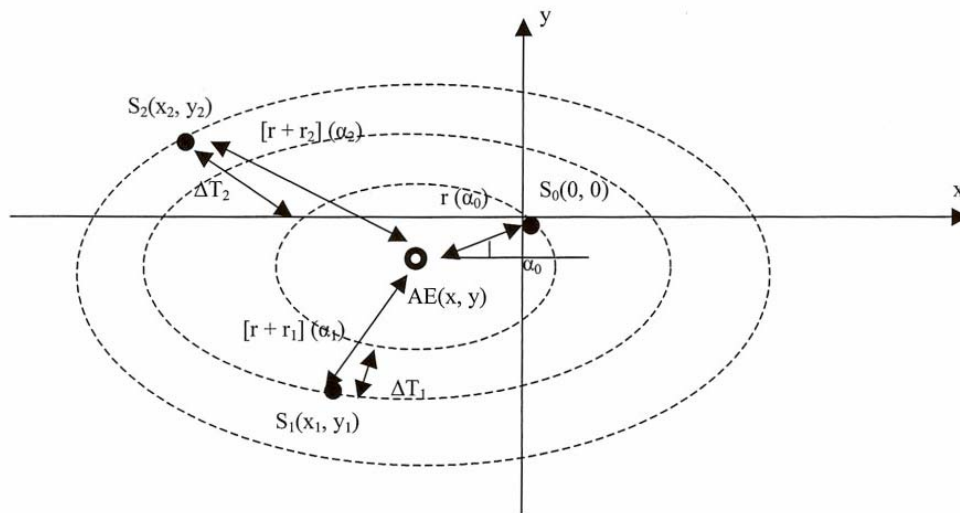
Figuren viser triangulerings – princippet ved elliptisk udbredelse.
Afstanden r er afhængig af vinklen α.

Den elliptiske udbredelse kan beskrives som et polynomium i 4 grad.
Y koordinaten fås af:

$$ay^4 + by^3 + cy^2 + dy + e = 0$$

Hvor *a, b, c, d, e* er defineret som:

$$a := \delta^2 - 16 \cdot \kappa \cdot \phi^4$$

$$b := 2 \cdot \delta \cdot \varepsilon + 16 \cdot \kappa \cdot \phi^4 \cdot (y_1 + y_2)$$

$$c := 2 \cdot \delta \cdot \xi + \varepsilon^2 - 16 \cdot y_1 \cdot y_2 \cdot \kappa \cdot \phi^4 + 4 \cdot \kappa \cdot \phi^2 \cdot (\tau_1 + \tau_2)$$

$$d := 2 \cdot \varepsilon \cdot \xi - 4 \cdot \kappa \cdot \phi^2 (\tau_1 \cdot y_2 + \tau_2 \cdot y_1)$$

$$e := \xi^2 - \kappa \cdot \tau_1 \cdot \tau_2$$

Og δ, ε, ξ er defineret som:

$$\begin{pmatrix} \delta \\ \varepsilon \\ \xi \end{pmatrix} := \begin{pmatrix} \chi^2 \\ 2 \cdot \rho \cdot \chi \\ \rho^2 \end{pmatrix} - (2 \cdot \phi \cdot v0)^2 \cdot \begin{bmatrix} -1\left[\tau_2 \cdot (\Delta T_2)^2\right] & -1\left[\tau_1 \cdot (\Delta T_1)^2\right] \\ y_2\left[\tau_2 \cdot (\Delta T_2)^2\right] & y_1\left[\tau_1 \cdot (\Delta T_1)^2\right] \\ \dfrac{\tau_2}{4 \cdot (\phi)^2}\left[\tau_2 \cdot (\Delta T_2)^2\right] & \dfrac{\tau_1}{4 \cdot (\phi)^2}\left[\tau_1 \cdot (\Delta T_1)^2\right] \end{bmatrix} \cdot \begin{pmatrix} \alpha_1 \\ \alpha_2 \end{pmatrix}$$

Yderligere er α, Φ, τ, κ defineret som:

$$\alpha_i := (\Delta T_i \cdot v0)^2 - (x_i)^2$$

$$\phi := \frac{v0}{v90}$$

$$\tau_i := \alpha_i - (\phi \cdot y_i)^2$$

$$\kappa := 4 \cdot \tau_1 \cdot \tau_2 \cdot \left[\alpha_1 \cdot \alpha_2 \cdot \Delta T_1 \cdot \Delta T_2 \cdot (v0)^2\right]^2$$

Og ρ, χ er defineret som:

$$\begin{pmatrix} \rho \\ \chi \end{pmatrix} := \begin{pmatrix} x_2 \cdot \tau_2 & -x_1 \cdot \tau_1 \\ x_2 \cdot y_2 & -x_1 \cdot y_1 \end{pmatrix} \cdot \begin{pmatrix} \alpha_1 \\ \alpha_2 \end{pmatrix}$$

Φ er forholder mellem lydhastighederne i x retningen $v(0^o)$ samt y retningen $v(90^o)$. ΔT_1 samt ΔT_2 er tidforskellen mellem 1st ramte sensor S_o samt henholdsvis sensor S_1 og S_2.

X koordinaten findes således ved at anvende de reelle losninger fra (1) som indsættes i ligning (2):

$$x = x_i\,(\tau_i + 2y_i\,\phi^2 y) \pm \Delta T_i \cdot v(0^o) \cdot (\tau_i(\tau_i + 4\,\phi^2(y_i - y))y)^{1/2}$$

Løsningen er den reelle rod hvor $AE(x,y)$ har den korteste distance til S_o (x,y).

Trianguleringssystemet

Trianguleringen foretages ved hjælp af et 4 kanalers dataopsamlingskort med samplingsfrekevens på 1 MHz pr. kanal. Kanalerne optager signalerne parallelt, så der ingen tidsforskydeise er på optagelsen. Når et signal rammer trigger kanalen aflæses alle 4 kanaler og gemmes som binær fil på en PC. Når optagelserne er færdig indlæses den binære fil i triangulatoren, hvor input er de relative koordinater på

sensorerne, lydhastigheden i x og y retningen samt divisionsfaktoren på high - low amplituden. Output er placering af de beregnede hits. Der foretages ligeledes en relativ energi differentiering af signalernes energiindhold. Dette betyder at systemet beregner en sandsynlig størrelse på energiudladningen i det lokaliserede område. På denne vis kan det estimeres hvor alvorlig skaden er.

Signalbehandlingen

Hvert signal består af 500 punkter, der tilsammen udgør signalkarakteristikken eller bølgeformen. Bølgeformen sendes gennem et Hanning filter for at blødgøre signalet. Der har været gode internationale erfaringer med at foretage denne filtrering indenfor AE teknologi. Bølgeformen udstrækker sig over 0,5ms og derfor kan den karakteriseres som en transient. På transienter er Hilbert algoritmen velegnet til [2] at udfolde signalet til en meningsfuld karakteristik, og derved kan signalet integreres og det relative energiindhold kan beregnes. Systemet optager med 4 kanaler og kun 3 skal bruges til beregning af placeringen af signalets udgangspunkt. Derfor udvælges de 3 signaler med det højeste energiindhold, derved fås de mest optimale betingelser for uddragningen af tidskoordinaterne.

Risø's research is aimed at solving concrete problems in the society.

Research targets are set through continuous dialogue with business, the political system and researchers.

The effects of our research are sustainable energy supply and new technology for the health sector.

www.risoe.dk